SiO and H$_2$O Maser Observations of Red Supergiants in Star Clusters Embedded in the Galactic Disk

Shuji DEGUCHI,[1] Jun-ichi NAKASHIMA,[2] Yong ZHANG,[2] Selina S. N. CHONG,[2] Kazutaka KOIKE,[1] and Sun KWOK[2]

[1]*Nobeyama Radio Observatory, National Astronomical Observatory, and Graduate University for Advanced Studies,*
Minamimaki, Minamisaku, Nagano 384-1305
[2]*Department of Physics, University of Hong Kong, Pokfulam Rd., Hong Kong, China*

Abstract

We present the results of radio observations of red supergiants in a star cluster, Stephenson (1990, AJ, 99, 1867)'s #2, and of candidates for red supergiants in three star clusters, Mercer et al. (2005, ApJ, 635, 560)'s #4, #8, and #13, in the SiO and H$_2$O maser lines. The Stephenson's #2 cluster and nearby aggregation at the southwest contain more than 15 red supergiants. We detected one red supergiant at the center of Stephenson's #2 and three in a southwest aggregation in the SiO maser line; three out of these four were also detected in the H$_2$O maser line. The average radial velocity of the four detected objects is 97 km s^{-1}, giving a kinematic distance of 5.5 kpc, which locates this cluster near the base of the Scutum–Crux spiral arm. We also detected six SiO emitting objects associated with other star clusters. In addition, mapping observations in the CO $J = 1$–0 line toward these clusters revealed that an appreciable amount of molecular gas still remains around the Stephenson's #2 cluster in contrast to the prototypical red-supergiant cluster, Bica et al. (2003, A&A, 404, 223)'s #122. This indicates that the time scale of gas expulsion differs considerably in individual clusters.

Key words: Galaxy: open clusters and associations: individual (Mercer et al.'s #4, #8, #13; Stephenson's #2), — masers — stars: mass-loss — stars: supergiants

1. Introduction

Massive young star clusters occasionally harbor a number of red supergiants with an initial mass of ~ 10–15 $M_\odot$ (Schild 1970), which are destined for a supernova explosion leaving behind a neutron star as a final product (Heger et al. 2003). Since red supergiants exhibit high luminosity, they are easily identified at infrared wavelengths, even if large interstellar extinction is assumed. They can be used as indicators of age and mass of star clusters embedded in the Galactic disk (Lada & Lada 2003; Figer et al. 2006). A red supergiant with $L = 10^5 L_\odot$ has a progenitor mass of $\sim 15 M_\odot$ (Salasnich et al. 1999), which is likely to be the upper limit of the initial masses of red supergiants in star clusters.

Figer et al. (2006) measured the equivalent widths of the CO first overtone bands, and identified fourteen M supergiants in a cluster in Scutum [#122 of Bica et al. (2003) = RSGC1]. They inferred that the initial mass and age of this cluster are ~ 2–4 $\times 10^4 M_\odot$ and 7–12 Myr, respectively, based on a color–luminosity diagram, assuming Salpeter's initial mass function. Nakashima and Deguchi (2006) detected SiO masers from four of these red supergiants. They found that the velocity dispersion of the maser sources is equivalent to that of a cluster with a mass of $\sim 10^4 M_\odot$, and that the average radial velocity of maser sources indicates a kinematic distance of 6.5 kpc to the cluster. This example demonstrated that SiO masers are a useful tool for studying the kinematics of star clusters as well as the mass-losing process of massive stars at the final stage of stellar evolution.

In this paper, we present the results of SiO and H$_2$O maser searches for red supergiants in Stephenson (1990)'s #2

(hereafter, Stephenson #2), and candidates for red supergiants in the other star clusters in the Mercer et al. (2005)'s catalog. The former cluster contains more than 10 red supergiants (Stephenson 1990). A later near-infrared (NIR) study found more supergiants and early type stars in the Stephenson #2 cluster (Nakaya et al. 2001). More recently, Davies et al. (2008) spectroscopically identified 15 red supergiants in the Stephenson #2 cluster and nearby aggregation 5′ southwest from the Stephenson #2 cluster. Mercer et al. (2005) cataloged ~ 200 infrared star clusters lying in the Galactic disk using the Spitzer/GLIMPSE survey. Some of them include nearby bright middle-infrared (MIR) sources, which are likely to be red supergiants showing a typical color of SiO maser sources. However, since the color ranges of evolved stars in the NIR and MIR bands somewhat overlap with those of young stellar objects, it is not easy to discriminate young stars from evolved stars solely based on the infrared colors. Detections of SiO masers are crucial in confirming the supergiant status of candidate stars in embedded clusters. We selected three star clusters (#4, #8, and #13) as observing targets from the Mercer et al. (2005)'s catalog; each selected cluster includes multiple candidates for red supergiants. Cluster #13 of Mercer et al. (2005), which is located $\sim 6°$ north of Stephenson #2, is interesting because of an associated bright IR object (144 Jy at 12 μm).

We also mapped the CO emission of Stephenson #2 and several other clusters selected from the Mercer et al.'s catalog. In addition, we mapped CO emission toward a prototypical red-supergiant star cluster in Scutum (RSGC1) for comparison. Massive star clusters are formed in giant molecular clouds (Lada & Lada 2003), but the gas components of the clusters are eventually expelled and dissociated by the radiation of massive

stars, while the stars are at the main sequence of stellar evolution, and at the later phase by supernova explosion (Lada et al. 1984). The dynamical evolution and dissolution of star clusters depend strongly on the gas expulsion process (see, e.g., Boily & Kroupa 2003). Therefore, it is interesting to know how much CO gas remains in the star clusters with red supergiants.

2. Observations and Results

The observations were made with the 45m radio telescope at Nobeyama in 2006 April and 2008 April in the H_2O $J_{KK} = 6_{16}–5_{23}$ transition at 22.235 GHz, the SiO $J = 1–0$ $v = 1$ transition at 43.122 GHz and $v = 2$ at 42.821 GHz, and the CO $J = 1–0$ transition at 115.271 GHz. Cooled HEMT receivers, H22 and H40, were used for the 22 GHz and 43 GHz observations with acousto-optical spectrometer arrays with the 40 and 250 MHz bandwidths, velocity resolutions of which are ~ 0.6 km s^{-1} at 22 GHz (0.3 km s^{-1} at 43 GHz) and 3.6 km s^{-1} at 22 GHz (1.8 km s^{-1} at 43 GHz), respectively. The overall system temperatures were ~ 140 K for the 22 GHz H_2O observations, and 180–250 K for the 43 GHz SiO. The half-power telescope beam widths (HPBW) were $\sim 90''$ at 22 GHz and $40''$ at 43 GHz. The conversion factors of the antenna temperature to the flux density were ~ 3.0 Jy K^{-1} at 22 GHz, and 2.9 Jy K^{-1} at 43 GHz. All of the observations were made in the position-switching mode. Since the sources in the clusters are concentrated in a small region of less than a $15' \times 15'$ area, we employed such a position-switching sequence as Off–On1–On2–On3, where the off position was taken $7'$ west of the first on-source position. This saves 50% of the integration time compared with a usual Off–On sequence (Deguchi et al. 2004a). The 5×5 beam focal-plane array receiver system (BEARS) was used for the 115 GHz CO observation (i.e., Sunada et al. 2000). The system temperatures of the array receivers were between 400 and 600 K (DSB). The grid spacing of the array receiver was $41''$ and the individual beam size was $\sim 15''$ (HPBW). The 1024 channel digital autocorrelator spectrometer (Sorai et al. 2000) with a band width of 32 MHz was used for the 115 GHz observations, giving an effective velocity resolution of 0.16 km s^{-1} in a two-channel binding mode. Further details of the observations with the NRO 45 m telescope have been described elsewhere,[1] and are not repeated here.

The data reductions were made by using the NEWSTAR software package developed by Nobeyama Radio Observatory. The BEARS data were first multiplied by the conversion factors of the antenna temperature for each beam displacement, and were integrated over time. Then, the best-fit quadratic curve was subtracted to determine a baseline of each spectrum. Channel maps were created by using the "MAP" task of NEWSTAR, with a separation of 2 km s^{-1} and a taper of 5 km s^{-1} for channel smoothing. The resulting CO channel maps are shown in figures 5a–5f.

Targets for SiO searches were chosen as follows. We first selected MIR objects brighter than 1 Jy in the MSX band C (12 μm) (Egan et al. 2003)[2] toward the Stephenson #2 and the Mercer et al.'s clusters. Since we noticed an aggregation of

bright MIR objects $5'$ southwest of Stephenson #2, we selected objects from a relatively large area ($1000'' \times 1000''$) covering both Stephenson #2 and the southwest aggregation, though some of them were possibly not a member of the cluster. We call the southwest aggregation "Stephenson #2 SW", hereafter. We then checked to see if the selected MIR objects had a NIR counterpart in a particular color range of the 2MASS colors[3] (Skrutskie et al. 2006) (i.e., $K < 9$ and $H - K > 0.9$), which have been used as criteria for target selections for our previous SiO maser surveys (Deguchi et al. 2004b). Finally, we selected 18 infrared objects in the Stephenson #2 and #2 SW clusters. The positions of the selected objects are shown in figure 1a.

The star clusters with red supergiants other than the Stephenson #2 were chosen from a table of new star clusters discovered in the GLIMPSE survey data [table 1 of Mercer et al. (2005)]. We selected the MIR objects using the same criteria as we mentioned above. Then, we eliminated several young stellar objects from this list conducting visual inspection of 2MASS images. For example, the objects associated with large extended nebulosity (e.g., Mercer et al.'s #40) were discarded. We selected three star clusters, including 15 candidates for red supergiants. In the case of Mercer et al.'s #4, we added three red stars (J18202853−1602159, J18204070−1603412, and J18203850−1604163), which do not fulfill the criteria, but facilitate our observing method using a three-on-point sequence. Table 1 summarizes the infrared properties of the observed sources. Figure 1 shows Spitzer/GLIMPSE images of the clusters and the positions of the observed objects. The star clusters, Mercer et al.'s #4 and #8, are rather hard to recognize on the GLIMPSE images shown in figures 1b and 1c, respectively, because of the scales, but they can be clearly seen on enlarged 2MASS images, which are not shown here. For convenience, we gave each star cluster such a short name, as an abbreviated cluster name and a star number separated by a hyphen, e.g., St2-01. Here, the Stephenson #2 cluster is designated by St2 (including St #2 SW), and Mercer et al.'s #4, #8, and #13 clusters are done by Mc4, Mc8, and Mc13, respectively. Table 4 summarizes the other names of these objects.

Table 2 summarizes the observational results of SiO masers, and table 3 those of H_2O masers. Figures 2a and 2b show the SiO and H_2O maser spectra of detected sources, respectively. Figure 3 shows the K magnitude versus NIR color and the 12 μm flux density versus MIR color diagrams, where the detections and nondetections are presented by filled and open circles, respectively. Note that the beam size of the telescope in the 22 GHz H_2O maser observation is $90''$ (HPBW), approximately twice larger than the beam size in the 43 GHz SiO observation. Since the mean angular distance between red supergiants in clusters is roughly $40''–50''$, we occasionally detected nearby H_2O maser sources that are contaminated through the Gaussian tail of the telescope beam. However, such contamination could be identified in the present observations, because we observed multiple, close positions within one cluster. The data give positional information about contaminating sources.

---

[1] See ⟨http://www.nro.nao.ac.jp/nro45mrt/obs/bears⟩.

[2] ⟨http://vizier.u-strasbg.fr/viz-bin/VizieR?-source=V/114⟩.

[3] Explanatory Supplement to the 2MASS All Sky Data Release and Extended Mission Products ⟨http://www.ipac.caltech.edu/2mass/releases/allsky/doc/explsup.html⟩.
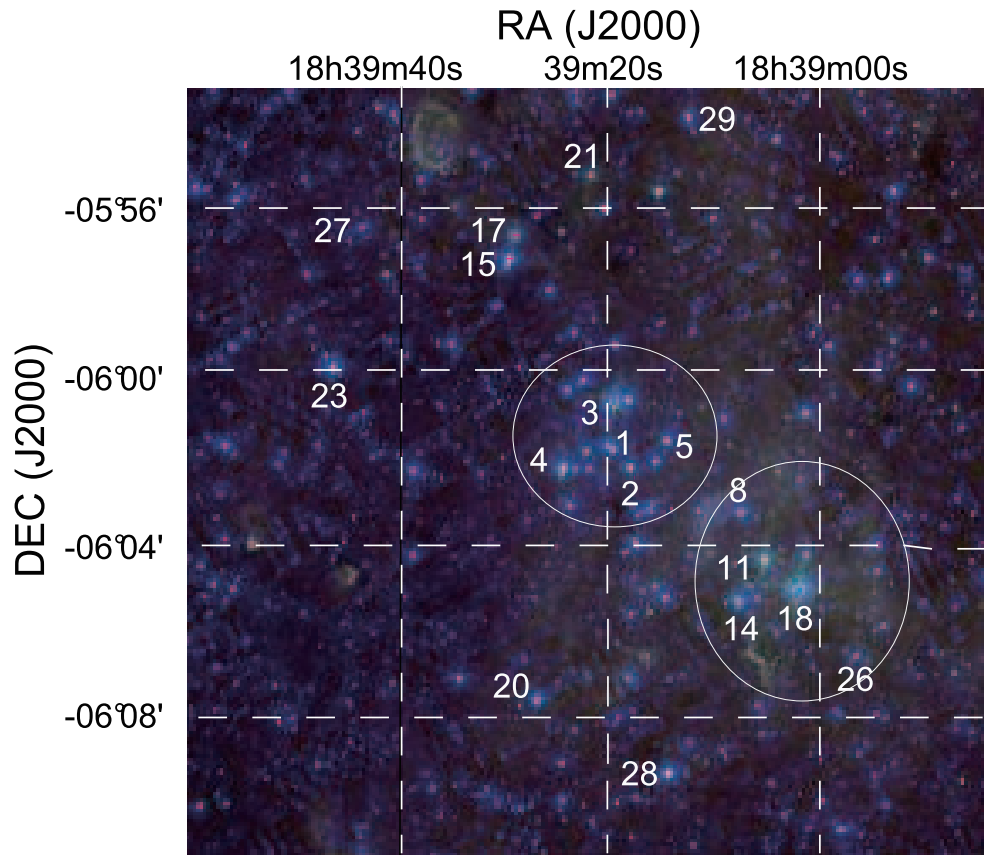
Fig. 1. (a) Positions of the observed sources overlaid on the Spitzer/GLIMPSE image of Stephenson #2. The two large ellipses indicate approximate positions of the clusters, Stephenson #2 (left) and #2 SW (right).
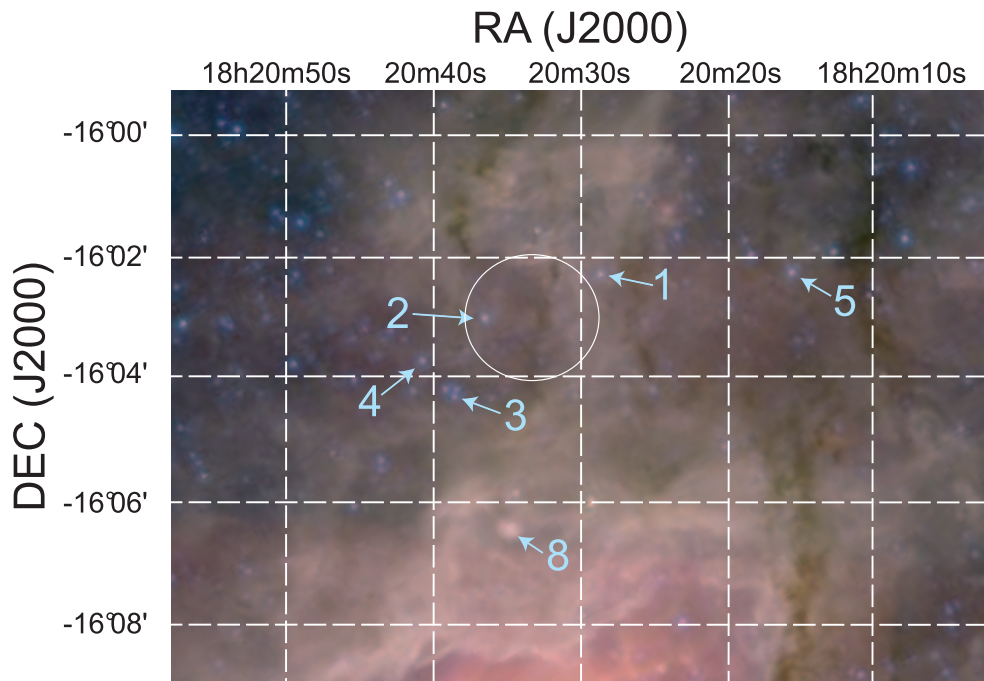

Fig. 1. (b) Positions of the observed sources overlaid on the Spitzer/GLIMPSE image of Mercer et al.'s #4 (shown by ellipse).
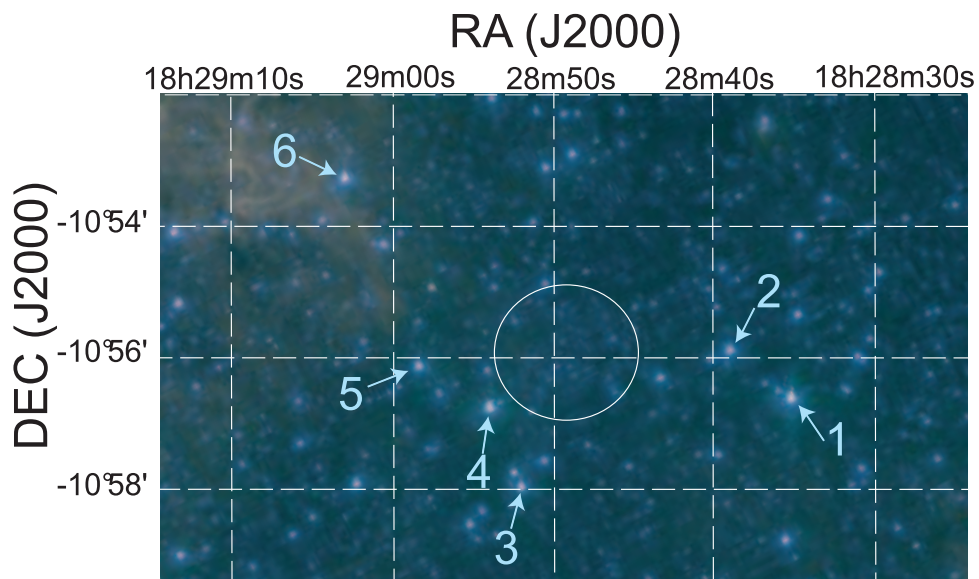
Fig. 1. (c) Positions of the observed sources overlaid on the Spitzer/GLIMPSE image of Mercer et al.'s #8 (shown by ellipse).
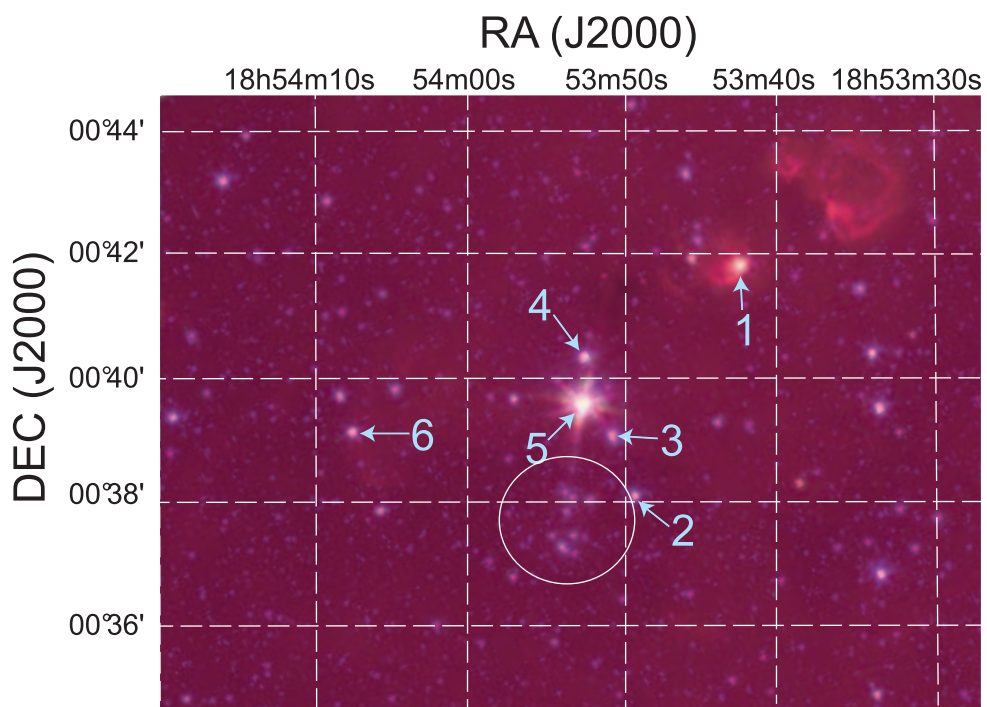

Fig. 1. (d) Positions of the observed sources overlaid on the Spitzer/GLIMPSE of Mercer et al.'s #13 (shown by ellipse).

Table 1. Properties of observed objects in Stephenson and embedded clusters.

2MASS name	No*	K	$J-H$	$H-K$	MSX name	Sepn. ('')	F_C (Jy)	C_{AC}	C_{CE}	V_{lsr}^{SiO} (km s^{-1})
18201544−1602142	Mc4-05	8.23	4.19	2.32	G015.1542−00.5707	0.8	2.2	0.408	0.034	—
18202853−1602159	Mc4-01	7.38	3.50	1.86	—	—	—	—	—	—
18203460−1606282	Mc4-08	8.89	2.35	1.63	G015.1288−00.6717	3.0	10.9	0.150	0.917	—
18203644−1602589	Mc4-02	7.98	4.04	2.26	G015.1831−00.6482	8.6	2.4	0.407	−0.247	18.3
18203850−1604163	Mc4-03	7.85	2.58	1.27	—	—	—	—	—	—
18204070−1603412	Mc4-04	7.70	2.86	1.39	—	—	—	—	—	—
18283530−1056364	Mc8-01	4.88	1.92	1.10	G020.6034+00.0234	0.4	5.6	0.081	−0.184	74.1
18283912−1055526	Mc8-02	4.97	1.89	0.89	G020.6214+00.0151	1.1	1.0	−0.091	−0.154	—
18285207−1057576	Mc8-03	6.23	2.23	1.32	G020.6156−00.0476	1.7	4.1	0.085	−0.105	102.4
18285402−1056453	Mc8-04	5.59	2.40	1.32	G020.6367−00.0452	0.3	3.6	0.055	−0.250	—
18285844−1056069	Mc8-05	5.57	2.08	1.23	G020.6545−00.0562	0.9	2.2	0.179	−0.329	108.6
18290303−1053153	Mc8-06	4.49	1.59	0.76	G020.7053−00.0511	1.0	2.3	−0.035	−0.482	—
18385699−0606459	St2-26	6.95	3.51	1.57	G026.0708−00.0208	7.6	1.8	0.124	—	92.3
18390238−0605106	St2-18	2.90	2.45	1.80	G026.1044−00.0283	5.6	56.9	0.260	−0.202	92.7
18390558−0604265	St2-11	7.32	4.31	2.60	G026.1215−00.0345	4.5	16.6	0.354	−0.067	98.6
18390776−0603203	St2-08	5.23	2.26	1.08	G026.1431−00.0343	3.4	1.5	0.049	—	—
18390805−0605244	St2-14	4.82	2.48	1.23	G026.1120−00.0510	4.7	4.9	0.159	−0.219	—
18391223−0553586	St2-29	6.47	3.53	1.77	G026.2891+00.0206	7.9	1.6	0.153	0.047	—
18391470−0601366	St2-05	5.24	2.00	0.97	G026.1806−00.0465	1.4	1.5	−0.051	—	—
18391489−0609272	St2-28	5.60	3.07	1.61	G026.0649−00.1076	7.8	3.4	0.121	−0.289	—
18391825−0602142	St2-02	5.26	2.15	0.95	G026.1782−00.0641	0.7	1.5	−0.042	—	—
18391961−0600408	St2-03	4.12	1.85	0.93	G026.2038−00.0574	1.0	19.9	0.180	−0.179	102.7
18391989−0601481	St2-01	5.11	1.80	0.91	G026.1886−00.0679	0.0	1.9	−0.021	—	—
18392161−0555197	St2-21	8.86	1.99	2.76	G026.2868−00.0240	6.3	2.7	0.158	−0.152	—
18392461−0602138	St2-04	4.50	1.82	0.96	G026.1903−00.0876	1.1	6.6	0.088	−0.401	—
18392736−0607408	St2-20	5.45	2.85	1.50	G026.1150−00.1395	6.2	3.4	0.223	−0.210	—
18392891−0556435	St2-17	5.82	2.07	1.25	G026.2800−00.0617	5.4	5.5	0.053	−0.209	50.2
18392947−0557165	St2-15	4.65	2.20	1.06	G026.2732−00.0679	4.9	5.4	0.135	−0.206	—
18394340−0556290	St2-27	5.88	1.95	0.90	G026.3112−00.1130	7.7	3.1	0.716	—	—
18394635−0559473	St2-23	4.51	1.71	0.83	G026.2678−00.1492	6.7	5.9	0.115	−0.126	—
18534227+0041459	Mc13-1	9.51	4.21	3.29	G033.8104−00.1869	2.5	18.8	0.348	0.470	—
18534913+0038021	Mc13-2	6.13	2.81	1.46	G033.7671−00.2406	1.3	—	—	—	—
18535060+0039015	Mc13-3	6.01	2.68	1.27	—	—	—	—	—	—
18535240+0040172	Mc13-4	5.89	3.67	1.95	G033.8071−00.2351	1.5	3.6	0.103	−0.216	—
18535249+0039313	Mc13-5	2.67	3.03	1.62	G033.7963−00.2417	1.6	144.9	0.184	−0.257	72.3
18540749+0039039	Mc13-6	7.28	2.87	1.66	G033.8179−00.3008	1.0	3.2	0.079	−0.101	73.3

* Star number in figure 1.

2.1. Stephenson #2

Several bright objects are identified with IRAS sources; the brightest two sources are IRAS 18366−0603 (St2-03) with $F_C = 19.9$ Jy and 18363−0607 (St2-18) with $F_C = 56.9$ Jy, and three others are IRAS 18364−0605 (St2-08), 18368−0610 (St2-20), and 18370−0602 (St2-23). However, the other fainter sources have no IRAS counterpart. Though St2-26 is a faint object with $F_C = 1.8$ Jy, we detected SiO maser emission. The broad-line profile of St2-18 suggests that this is a typical red supergiant (e.g., Cernicharo et al. 1997).

The radial velocity of St2-17 is shifted by more than 40 km s^{-1} from the velocities of the other stars. Therefore, we conclude that St2-17 is not a member of Stephenson #2. From this we infer that some stars in the northeastern part

of Stephenson #2 (i.e., St2-15, St2-21, St2-23, St2-27, and St2-29) (figure 1a), which are located far from the cluster center, are not physically associated with Stephenson #2.

It is interesting to us whether or not Stephenson #2 SW is physically associated with Stephenson #2. Note that Stephenson #2 includes St2-01 to St2-05, and Stephenson #2 SW does St2-08, St2-11, St2-14, St2-18, and St2-26. The angular size of Stephenson #2 suggested by Bica et al. (2003) is $3'.5 \times 3'$, and Stephenson #2 SW is on the outside of this area. The averages of radial velocities and velocity dispersions for the SiO sources in Stephenson #2 SW are 94.5 km s^{-1} and 3.5 km s^{-1}, respectively. The former is shifted from the velocity of St2-3 in the Stephenson #2 by 8.2 km s^{-1}. This difference is not large enough to rule out any association of Stephenson #2 SW with Stephenson #2. For convenience,

Table 2. Observational results of the SiO maser search.

| 2MASS name | No* | SiO $J = 1$–0 $v = 1$ | | | | SiO $J = 1$–0 $v = 2$ | | | | Obs. date |
		T_a (K)	V_{lsr} (km s^{-1})	L.F. (K km s^{-1})	rms (K)	T_a (K)	V_{lsr} (km s^{-1})	L.F. (K km s^{-1})	rms (K)	(yymmdd.d)
18201544−1602142	Mc4-05	—	—	—	0.049	—	—	—	0.052	080427.2
18202853−1602159	Mc4-01	—	—	—	0.038	—	—	—	0.036	080428.2
18203460−1606282	Mc4-08	—	—	—	0.051	—	—	—	0.055	080427.2
18203644−1602589	Mc4-02	0.210	18.3	0.542	0.037	—	—	—	0.035	080428.2
18203850−1604163	Mc4-03	—	—	—	0.051	—	—	—	0.056	080427.2
18204070−1603412	Mc4-04	—	—	—	0.037	—	—	—	0.035	080428.2
18283530−1056364	Mc8-01	0.932	74.6	3.285	0.051	0.673	73.7	2.601	0.053	080427.2
18283912−1055526	Mc8-02	—	—	—	0.046	—	—	—	0.048	080427.2
18285207−1057576	Mc8-03	0.312	101.9	0.826	0.052	0.311	102.9	0.927	0.050	080427.2
18285402−1056453	Mc8-04	—	—	—	0.048	—	—	—	0.050	080427.2
18285844−1056069	Mc8-05	0.221	108.6	0.374	0.050	0.273	108.6	0.846	0.054	080427.2
18290303−1053153	Mc8-06	—	—	—	0.046	—	—	—	0.050	080427.2
18385699−0606459	St2-26	0.258	94.2	0.589	0.065	0.330	90.4	0.582	0.068	060415.3
18390238−0605106	St2-18	0.367	92.7	4.199	0.062	—	—	—	0.065	060412.3
18390558−0604265	St2-11	1.963	100.9	16.398	0.072	1.378	96.3	8.621	0.066	060412.3
18390776−0603203	St2-08	—	—	—	0.075	—	—	—	0.074	060413.3
18390805−0605244	St2-14	—	—	—	0.064	—	—	—	0.067	060412.3
18391223−0553586	St2-29	—	—	—	0.068	—	—	—	0.067	060415.3
18391470−0601366	St2-05	—	—	—	0.070	—	—	—	0.075	060413.3
18391489−0609272	St2-28	—	—	—	0.068	—	—	—	0.068	060415.3
18391825−0602142	St2-02	—	—	—	0.072	—	—	—	0.072	060413.3
18391961−0600408	St2-03	0.435	102.7	0.726	0.074	—	—	—	0.074	060413.3
18391989−0601481	St2-01	—	—	—	0.071	—	—	—	0.071	060413.3
18392161−0555197	St2-21	—	—	—	0.083	—	—	—	0.087	060416.3
18392461−0602138	St2-04	—	—	—	0.074	—	—	—	0.075	060413.3
18392736−0607408	St2-20	—	—	—	0.066	—	—	—	0.068	060415.3
18392891−0556435	St2-17	0.345	49.1	0.979	0.070	0.193	51.3	0.809	0.069	060415.3
18392947−0557165	St2-15	—	—	—	0.085	—	—	—	0.085	060416.3
18394340−0556290	St2-27	—	—	—	0.070	—	—	—	0.068	060415.3
18394635−0559473	St2-23	—	—	—	0.086	—	—	—	0.087	060416.3
18534227+0041459	Mc13-1	—	—	—	0.042	—	—	—	0.044	080427.1
18534913+0038021	Mc13-2	—	—	—	0.033	—	—	—	0.042	080427.2
18535060+0039015	Mc13-3	—	—	—	0.045	—	—	—	0.044	080427.1
18535240+0040172	Mc13-4	—	—	—	0.040	—	—	—	0.042	080427.2
18535249+0039313	Mc13-5	0.993	69.4	10.487	0.080	—	—	—	0.077	060413.4
	Mc13-5	0.941	72.3	7.148	0.043	—	—	—	0.045	080427.1
18540749+0039039	Mc13-6	0.278	74.9	1.053	0.041	0.184	71.6	0.697	0.042	080427.2

* Star number in figure 1.

we presume that Stephenson #2 SW is associated with Stephenson #2.

2.2. Mercer et al.'s #4

This cluster is located at the northern boundary of M 17. SiO masers were detected only in Mc4-02 (J18203644−1602589) at $V_{lsr} = 18$ km s^{-1}. Water masers were detected at several locations. The radial velocity of Mc4-02, determined from the present SiO observation, is close to that of the CO component of M 17 at $V_{lsr} = 20$–23 km s^{-1} (Lada 1976). In fact, a strong CO emission is seen in the northwest parts of the channel maps in the range of $V_{lsr} = 20$–23 km s^{-1}. The H$_2$O maser emission was detected toward three objects: Mc4-01,

Mc4-03, and Mc4-08. Because of the large beam size at 22 GHz, H$_2$O emission of nearby objects could be detected at the tail of a Gaussian beam. The velocity of H$_2$O emission toward Mc4-03 is 20.5 km s^{-1}. This is close to the velocity 19.4 km s^{-1} of the secondary (redshifted) component of H$_2$O emission of Mc4-08. The angular distance between these two objects is 143″ (figure 1b), indicating that the intensity should be reduced to the 0.1% level if the 19.4 km s^{-1} emission from Mc4-08 is detected at the Gaussian tail of the beam pattern at the position of Mc4-03. The observed ratio of the integrated intensity of Mc4-03 to that of Mc4-08 is 29%, which is too large for a side-lobe detection, indicating that the 20.5 km s^{-1} emission of Mc4-03 is not a contamination

Table 3. Observational results of the H_2O maser search.

| 2MASS name | No* | H_2O $6_{16}-5_{23}$ | | | | Second peak | | | | Obs. date |
		T_a (K)	V_{lsr} (km s^{-1})	L.F. (K km s^{-1})	rms (K)	T_a (K)	V_{lsr} (km s^{-1})	L.F. (K km s^{-1})	rms (K)	(yymmdd.d)
18201544−1602142	Mc4-05	—	—	—	0.027	—	—	—	—	080430.1
18202853−1602159	Mc4-01	2.232	24.0	6.119	0.032	—	—	—	—	080430.1
18203460−1606282	Mc4-08	0.428	−44.5	0.803	0.028	0.209	19.4	0.684	—	080430.1
18203644−1602589	Mc4-02	—	—	—	0.031	—	—	—	—	080430.1
18203850−1604163	Mc4-03	0.101	20.5	0.201	0.027	—	—	—	—	080430.1
18204070−1603412	Mc4-04	—	—	—	0.035	—	—	—	—	080430.1
18283530−1056364	Mc8-01	—	—	—	0.033	—	—	—	—	080430.2
18283912−1055526	Mc8-02	—	—	—	0.071	—	—	—	—	080430.2
18285207−1057576	Mc8-03	—	—	—	0.034	—	—	—	—	080430.2
18285402−1056453	Mc8-04	—	—	—	0.074	—	—	—	—	080430.2
18285844−1056069	Mc8-05	—	—	—	0.039	—	—	—	—	080430.2
18290303−1053153	Mc8-06	—	—	—	0.099	—	—	—	—	080430.2
18385699−0606459	St2-26	—	—	—	0.035	—	—	—	—	080430.2
18390238−0605106	St2-18	0.519	95.6	7.368	0.031	—	—	—	—	080430.1
18390558−0604265	St2-11	2.610	87.2	28.605	0.032	—	—	—	—	080430.1
18390776−0603203	St2-08	0.167	86.7	1.583	0.031	—	—	—	—	080430.1
18390805−0605244	St2-14	—	—	—	0.032	—	—	—	—	080430.1
18391223−0553586	St2-29	—	—	—	0.033	—	—	—	—	080430.2
18391470−0601366	St2-05	—	—	—	0.031	—	—	—	—	080430.1
18391489−0609272	St2-28	—	—	—	0.033	—	—	—	—	080430.2
18391825−0602142	St2-02	—	—	—	0.030	—	—	—	—	080430.1
18391961−0600408	St2-03	0.112	106.8	0.336	0.034	—	—	—	—	080430.1
18391989−0601481	St2-01	—	—	—	0.032	—	—	—	—	080430.1
18392161−0555197	St2-21	—	—	—	0.033	—	—	—	—	080430.2
18392461−0602138	St2-04	—	—	—	0.035	—	—	—	—	080430.1
18392736−0607408	St2-20	—	—	—	0.042	—	—	—	—	080430.2
18392891−0556435	St2-17	—	—	—	0.033	—	—	—	—	080430.2
18392947−0557165	St2-15	—	—	—	0.034	—	—	—	—	080430.2
18394340−0556290	St2-27	—	—	—	0.037	—	—	—	—	080430.2
18394635−0559473	St2-23	—	—	—	0.035	—	—	—	—	080430.2
18534227+0041459	Mc13-1	2.476	45.4	5.225	0.032	—	—	—	—	080430.0
18534913+0038021	Mc13-2	—	—	—	0.032	—	—	—	—	080430.0
18535060+0039015	Mc13-3	0.717[‡]	70.2[‡]	2.163[‡]	0.034	—	—	—	—	080430.0
18535240+0040172	Mc13-4	0.445	21.4	0.950	0.031	0.635[‡]	70.2[‡]	1.858[‡]	—	080430.0
18535249+0039313	Mc13-5	1.495	70.2	5.011	0.036	0.197[†]	20.4[†]	0.404[†]	—	080430.0
18540749+0039039	Mc13-6	—	—	—	0.033	—	—	—	—	080430.0

* Star number shown in figure 1.
[†] Contamination from Mc13-4.
[‡] Contamination from Mc13-5.

from Mc4-08 (though we cannot rule out the possibility that the emission comes from an unknown H_2O source located near the middle point of Mc4-03 and Mc4-08). Two water maser sources (possibly of a young star origin) have been detected to the north of M 17 (Cesarsky et al. 1978; Braz & Epchtein 1983): G15.18−0.62 (+21 km s^{-1}) and G15.20−0.63 (+47 km s^{-1}). They are located at 20″ and 92″ away from Mc4-01 ($V_{lsr} = 24$ km s^{-1}). Therefore, G15.18−0.62 could be the same H_2O maser source as Mc4-01, but G15.20−0.63 is different from Mc4-01. The result that the peak velocities of Mc4-01 and G15.18−0.62 differ by 3 km s^{-1} could be explained by the time variation of a line profile. Thus, we conclude that two out of the three H_2O maser sources detected

in the present observation are new.

2.3. Mercer et al.'s #8

In Mc8-01, SiO maser emission was detected at $V_{lsr} = 74$ km s^{-1}, which is considerably different from the average velocity of Mc8-03 and Mc8-05 (105.5 km s^{-1}) (figure 1c). Therefore, it is possible that the object Mc8-01 is a foreground source. Since no water maser was detected toward this star cluster (table 3), dense molecular gas of a young star origin (as seen toward Mercer et al.'s #4) does not remain inside this star cluster. In fact, the CO channel maps shown in figure 5d indicate that CO emission is quite weak toward this cluster, except for the 106 km s^{-1} component, which extends
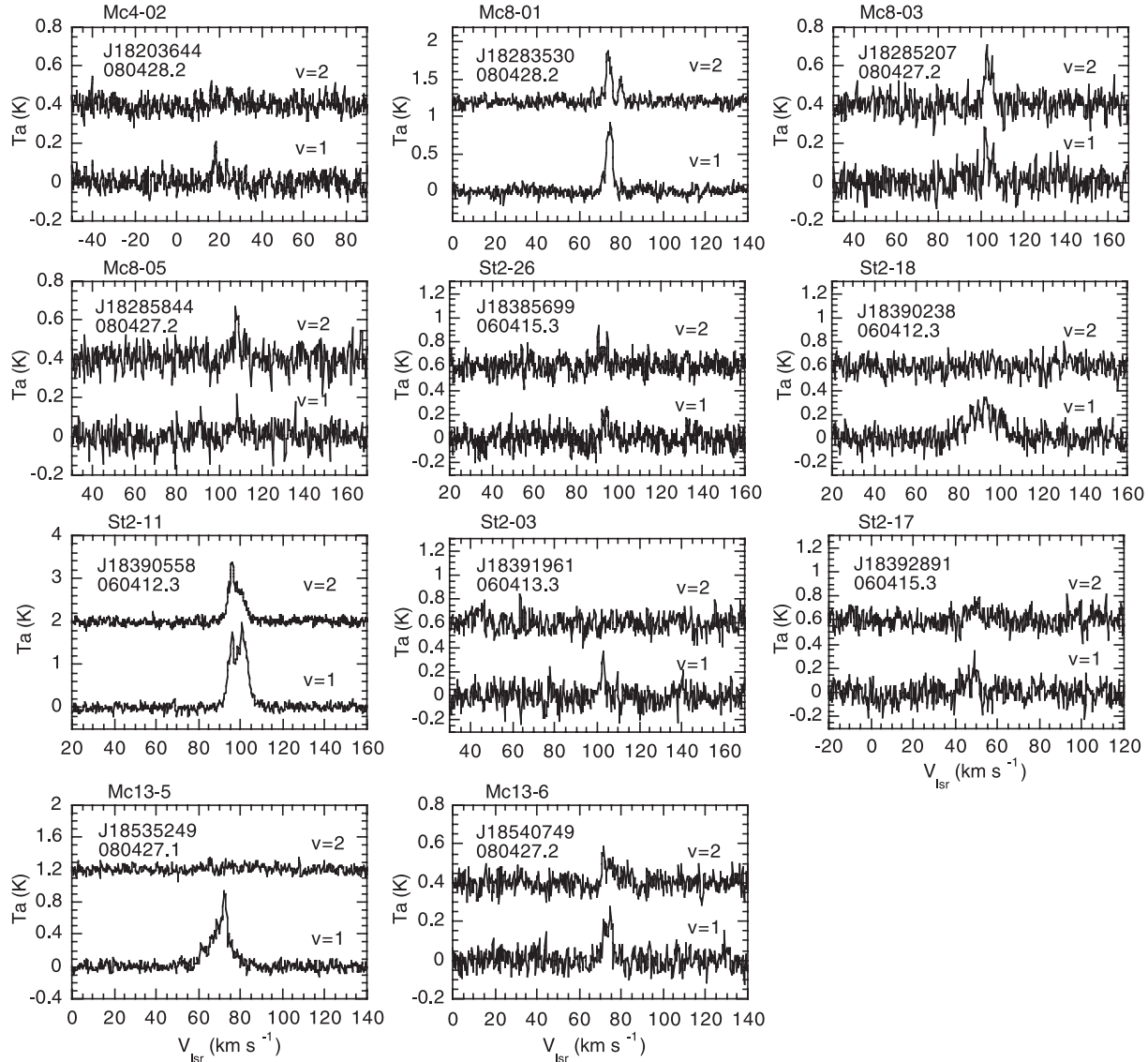
Fig. 2. (a) SiO $J = 1$–0 $v = 1$ and 2 spectra. The star name, abbreviation of 2MASS name (Jhhmmssss format), and the observed date (yymmdd.d format) are shown at the upper left of each panel.

through the northeast region of the star cluster toward Mc8-05. A pulsar, PSR J1828−1057, exists 1′ southeast of Mc8-01, and three X-ray sources (XGPS-I J182844−105428, XGPS-I J182851−105539, and GPSR5 20.722−0.075) exist in this direction. The presence of these high-energy sources seems to be consistent with the interpretation that CO gas was wiped out by supernova explosions.

2.4. Mercer et al.'s #13

Mc13-5 in this star cluster is a bright IR source ($F_C = 145$ Jy), but a search for SiO maser in this object was negative in a previous observation (Hall et al. 1990). We detected the SiO masers for the first time in this object. Water maser was detected toward Mc13-1, Mc13-3, Mc13-4, and Mc13-5. However, since the angular separation of Mc13-3 and Mc13-5 is only 41″ (figure 1d), the H_2O emission at $V_{lsr} = 70.2$ km s^{-1} detected at the position of Mc13-3 comes

from Mc13-5. Similarly, the angular distance between Mc13-4 and Mc13-5 is 46″; the emission at the position of Mc13-4 also suffers contamination from Mc13-5. The emission at $V_{lsr} = 21.4$ km s^{-1} detected toward Mc13-4 is stronger than that detected at the position of Mc13-5. Therefore, we conclude that the emission at 21.4 km s^{-1} is associated with Mc13-4. A compact CO emission at $V_{lsr} = 75$ km s^{-1} was found at a middle position between Mc13-5 and Mc13-6 (see figure 5e), indicating that the molecular gas still remains in this cluster.

2.5. Bica et al.'s #122 = RSGC1

In addition to the star clusters mentioned above, we observed CO emission toward Bica et al. (2003)'s #122 (= RSGC1 in Davies et al. 2007), which involves 14 red supergiants (Figer et al. 2006). SiO masers have been detected in four out of them (Nakashima & Deguchi 2006); the averages of
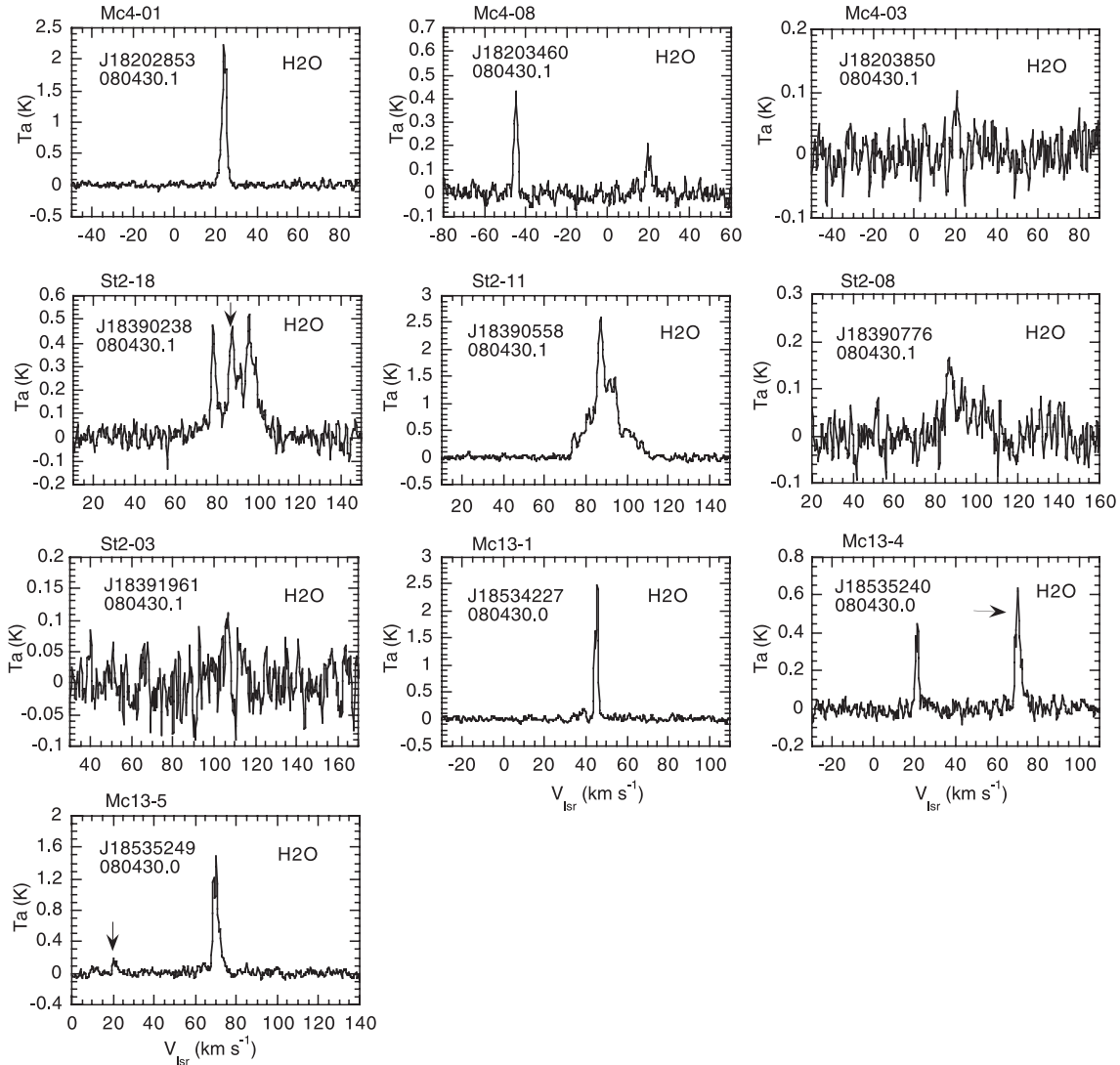
Fig. 2. (b) H_2O $6_{16}-5_{23}$ spectra. The star name, abbreviation of 2MASS name (Jhhmmssss format), and the observed date (yymmdd.d format) are shown at the upper left of each panel. The arrows indicate the emission contaminated from the other object detected at the Gaussian tail of the beam.

radial velocities and velocity dispersions are $120\,\mathrm{km\,s^{-1}}$ and $3\,\mathrm{km\,s^{-1}}$, respectively. The lower right panel of figure 4 shows the CO $J = 1$–0 spectra of Bica et al.'s #122 taken at five different positions aligning in the north–south direction (with the center of the star F13: Nakashima & Deguchi 2006). CO emission was seen in the velocity range of 85–110 $\mathrm{km\,s^{-1}}$. However, CO emission that is stronger than $T_a = 0.2\,\mathrm{K}$ was not detected at the velocity of above $110\,\mathrm{km\,s^{-1}}$ toward this cluster in this work. This fact suggests that almost no molecular gas remains in this cluster.

3. Discussion

We observed 36 candidates for red supergiants in four star clusters in the SiO and H_2O maser lines, and obtained their accurate radial velocities. The membership of stars in each cluster was confirmed by velocity information obtained in the present observation, since the velocities of contaminated background stars are generally different from those of member stars. With the velocity information obtained from the present maser observation, we can infer whether or not the CO emission is associated with the star cluster in terms of the radial velocities.

3.1. Cluster Kinematics of Stephenson #2

The age and distance of the Stephenson #2 cluster were somewhat uncertain. Nakaya et al. (2001) estimated the age to be 50 Myr and the distance 1.5 kpc, from a magnitude–color diagram. However, Ortolani et al. (2002) suggested an age of 20 Myr and a distance of 6 kpc for this cluster, based on the $VIJH$-band photometry and model calculations. The average of radial velocities (i.e., St2-03, St2-11, St2-18, and St2-26) obtained in the present observation is $96.6\,\mathrm{km\,s^{-1}}$, giving a kinematic distance of 5.5 kpc. This distance is consistent with an estimation given by Ortolani et al. (2002). Here, we assumed a flat rotation curve with a constant velocity of

Table 4. Other names for observed objects.

2MASS name	No*	D07[†]	MSX name	Other names & note
18201544−1602142	Mc4-05		G015.1542−00.5707	
18202853−1602159	Mc4-01		—	H$_2$O G15.18−0.62
18203460−1606282	Mc4-08		G015.1288−00.6717	M17WF 24[‡]
18203644−1602589	Mc4-02		G015.1831−00.6482	M17WF 26[‡]
18203850−1604163	Mc4-03		—	M17WF 29[‡]
18204070−1603412	Mc4-04		—	
18283530−1056364	Mc8-01		G020.6034+00.0234	IRAS 18258−1058
18283912−1055526	Mc8-02		G020.6214+00.0151	
18285207−1057576	Mc8-03		G020.6156−00.0476	
18285402−1056453	Mc8-04		G020.6367−00.0452	
18285844−1056069	Mc8-05		G020.6545−00.0562	
18290303−1053153	Mc8-06		G020.7053−00.0511	StRS 202
18385699−0606459	St2-26		G026.0708−00.0208	
18390238−0605106	St2-18	1	G026.1044−00.0283	IRAS 18363−0607 (17″)
18390558−0604265	St2-11	49	G026.1215−00.0345	K4
18390776−0603203	St2-08	9	G026.1431−00.0343	M5 IRAS 18364−0605 (26″)
18390805−0605244	St2-14	5	G026.1120−00.0510	M4
18391223−0553586	St2-29		G026.2891+00.0206	
18391470−0601366	St2-05	10	G026.1806−00.0465	M5
18391489−0609272	St2-28		G026.0649−00.1076	
18391825−0602142	St2-02	11	G026.1782−00.0641	M4
18391961−0600408	St2-03	2	G026.2038−00.0574	M3 Cl Stephenson 2 2, IRC −10447
18391989−0601481	St2-01	8	G026.1886−00.0679	K5 Cl Stephenson 2 4
18392161−0555197	St2-21		G026.2868−00.0240	
18392461−0602138	St2-04	3	G026.1903−00.0876	M4 Cl Stephenson 2 10
18392736−0607408	St2-20		G026.1150−00.1395	
18392891−0556435	St2-17	22	G026.2800−00.0617	
18392947−0557165	St2-15	4	G026.2732−00.0679	
18394340−0556290	St2-27		G026.3112−00.1130	
18394635−0559473	St2-23		G026.2678−00.1492	IRAS 18370−0602, StRS 239
18534227+0041459	Mc13-1		G033.8104−00.1869	IRAS 18511+0038
18534913+0038021	Mc13-2		G033.7671−00.2406	
18535060+0039015	Mc13-3		—	
18535240+0040172	Mc13-4		G033.8071−00.2351	
18535249+0039313	Mc13-5		G033.7963−00.2417	IRAS 18513+0035, NSV 11485
18540749+0039039	Mc13-6		G033.8179−00.3008	

* Star number in figure 1.
[†] Davies et al. (2007).
[‡] Ando et al. (2002).

220 km s^{-1} and a distance to the Galactic center of 8 kpc.

The standard deviation of radial velocities is 4.4 km s^{-1} (for 4 stars). To obtain this value, we assumed an uncertainty of 2 km s^{-1} in a velocity measurement of the SiO maser observation [see, subsection 3.2 in Nakashima & Deguchi (2006)]. The velocity dispersion gives a virial mass of the cluster ($\equiv 6\bar{r}\bar{v}_r^2/G$: Eigenbrod et al. 2004) of $1.3 \times 10^5 M_\odot$ under the assumption that the radius of the cluster (including both Stephenson #2 and Stephenson #2 SW) is 3′.1 (~ 5.5 pc). The obtained virial mass is larger than the mass of the Bica et al.'s #122 (2–$4 \times 10^4 M_\odot$: Figer et al. 2006). The virial mass only for Stephenson #2 SW is $3.7 \times 10^4 M_\odot$ for a radius of 2′ (3.5 pc). This value is close to the mass of Bica et al.'s #122, and seems to be reasonable for a single massive cluster.

Davies et al. (2007) obtained the K-band spectra of ~ 70 stars in Stephenson #2 and Stephenson #2 SW with the Kitt Peak National Observatory 4 m telescope. They measured equivalent widths of the CO band-head features and obtained the radial velocities by cross-correlating the band-head features with that of Arcturus. We compared the radial velocities obtained in the present radio observation with those obtained from the above-mentioned infrared observations [see figure 4 of Davies et al. (2007)]. The radio and infrared radial velocities of St2-18 [no. 1 of Davies et al. (2007)] coincide within ~ 2 km s^{-1}, but the other three stars do not show a good match in velocity, and the difference is roughly 8–10 km s^{-1}. On average, the radial velocities obtained from the CO band head are systematically redshifted by ~ 10 km s^{-1}. It has been
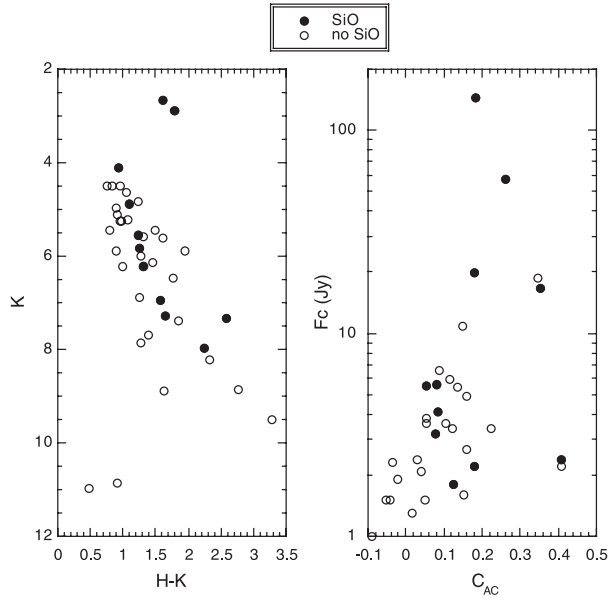
Fig. 3. K magnitude versus $H - K$ color and $12\,\mu\mathrm{m}$ flux density versus C_{AC} diagrams of the observed objects. Filled and open circles indicate SiO maser detections and nondetections, respectively.

known that the radial velocities obtained from infrared line profiles are systematically shifted from the true velocity of a star because of the scattering by dust grains in outflowing circumstellar envelopes (Reid & Dickinson 1976; Van Blerkom & Mao 1982). Therefore, if we take into account the uncertainty in the radial velocity obtained from the infrared observation, we can say that the velocities obtained in the present observation is consistent with those given by Davies et al. (2007).

3.2. CO Emission toward Stephenson #2

The CO channel maps in the velocity range of $V_{\mathrm{lsr}} = 101$–$105\,\mathrm{km\,s^{-1}}$ (figure 5a) show an emission enhancement near the center of the map (though the peak position does not coincide with the map center). The radial velocity of this cloud is approximately equal to the SiO radial velocity of St2-03 ($102.7\,\mathrm{km\,s^{-1}}$). Therefore, it is likely that this cloud is associated with the star cluster Stephenson #2. In contrast, the CO channel maps of Stephenson #2 SW (figure 5b) exhibit no strong enhancement of emission around the map center, but emission features are seen near the south edge of the map. Additionally, a weak emission peak is noticeable at the northeast part of the channel maps [(RA, Dec) $\sim$ (18$^{\mathrm{h}}$39$^{\mathrm{m}}$05$^{\mathrm{s}}$, $-06°04'30''$)] in the V_{lsr} range of 93–103 km s^{-1}. The coordinates and velocity of this component roughly coincide with those of St2-11. However, we attribute this CO emission to a fragment of the cloud toward this direction, which is not related to the circumstellar envelope of the red supergiant St2-11, because the CO intensity is too strong for a red supergiant 5 kpc away.

Jackson et al. (2006) mapped the region of $l = 18°$–$58°$ and $|b| < 1°$ in the ^{13}CO $J = 1$–0 radio line with the 22$''$ beam of on-the-fly sampling. Their channel map at $V_{\mathrm{lsr}} = 95$–$115\,\mathrm{km\,s^{-1}}$ exhibits an emission peak near Stephenson #2 at

$(l, b) \sim (26°15, -0°08)$. This position, possibly the densest part of the molecular cloud in this complex, is a few arcminutes south of Stephenson #2 and a few arcminutes east of Stephenson #2 SW, but it is outside of figures 1a and 1b. If we assume that the kinematic distance is reliable, the Stephenson #2 SW cluster ($V_{\mathrm{lsr}} \sim 94\,\mathrm{km\,s^{-1}}$) is located at this side of the Stephenson #2 complex, and the thick CO cloud with the spectral peak showing an intensity peak at $V_{\mathrm{lsr}} \sim 100$–$105\,\mathrm{km\,s^{-1}}$ is located at the far side. Furthermore, Stephenson #2 ($V_{\mathrm{lsr}} \sim 102\,\mathrm{km\,s^{-1}}$) is close to the thick CO cloud. This conjecture is consistent with the configuration of the Scutum–Crux arm, which has a tangency at a distance of 7 kpc from the Sun in the direction of $l \sim 35°$. The Scutum–Crux arm crosses the tip of the Bulge bar at a distance of ~ 6 kpc in the direction of $l \sim 30°$, approaching toward the Sun with decreasing l (see, e.g., Benjamin 2008). Therefore, the difference in radial velocity between Stephenson #2 and Stephenson #2 SW can be understandable in terms of the structure and kinematics of the Scutum–Crux arm.

3.3. CO toward the Bica et al.'s #122 and Comparison with Stephenson #2

A red-supergiant star cluster, Bica et al.'s #122 (RSGC1), is located very close to Stephenson #2 with a separation of $\sim 1°0$. No CO emission is seen toward Bica et al.'s #122 at the velocity of above $110\,\mathrm{km\,s^{-1}}$ in lower right panel of figure 4 and in figure 5f. This fact suggests that almost no molecular gas is left behind Bica et al.'s #122. This stands in a sharp contrast with the case of Stephenson #2 (RSGC2). The ages of red supergiants of Bica et al.'s #122 and Stephenson #2 were estimated to be 8 and 17 Myr, respectively, from isochrone fittings using the "fast-rotating" Geneva models. Davies et al. (2007) found that the ages of red supergiants in Stephenson #2 show a relatively large dispersion (several Myr), and therefore they concluded that the red supergiants in Stephenson #2 are not coeval with those in Stephenson #2 SW. For the case of Stephenson #2, the radial velocity obtained from the present SiO maser observation is slightly different from that obtained from the NIR observation. This fact suggests that the distance to Stephenson #2 and #2 SW clusters is shorter than the previous expectation. It is reasonably concluded that Stephenson #2 and #2 SW are located in front of the base of the Scutum–Crux arm (e.g., Russeil 2003), and that Bica et al.'s #122 is much farther than Stephenson #2; i.e., Bica et al.'s #122 is located near the tangent point of this direction, possibly inside the circle of the Galactic bulge tip. The aged cluster Stephenson #2 appears to hold more CO gases than the younger cluster Bica et al.'s #122 does. This fact seems to indicate that the gas expulsion from a star cluster is not a simple function of time, but depends on the environment of the cluster, possibly on a mass and sphericity of the original molecular cloud, a distribution of birth dates of massive stars, and a positioning of sequence of cloud formation in a spiral arm.

Note that the radial velocity of Stephenson #2 ($\sim 96\,\mathrm{km\,s^{-1}}$) falls on the "Molecular Ring" feature in the longitude–velocity map of the Galactic disk CO emission (see, Dame et al. 2001), but the velocity of Bica et al.'s #122 (120 km s^{-1}) exceeds the molecular ring velocity at $l = 26°$. This fact suggests that Bica et al.'s #122 is formed under a strong influence of the
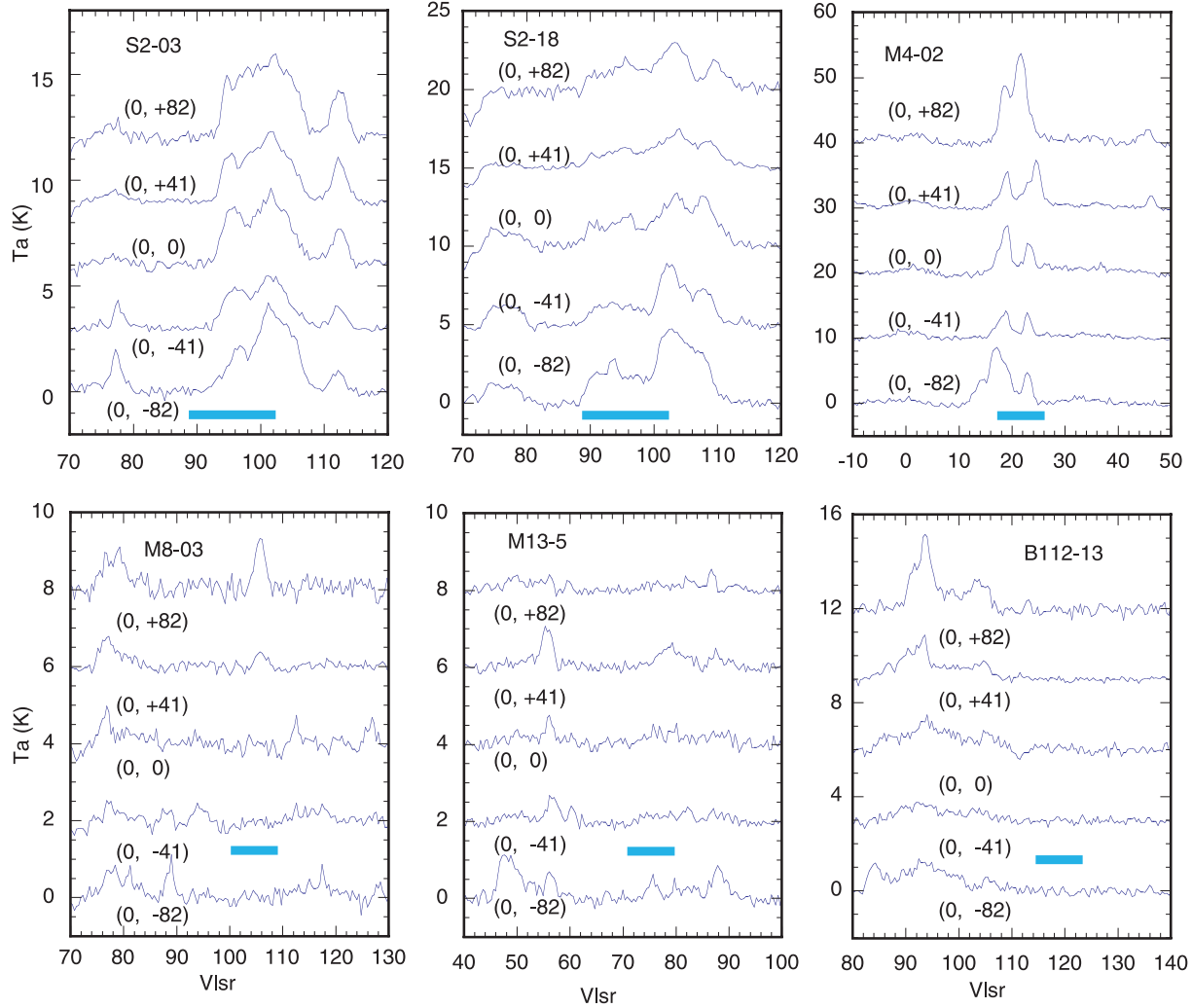
Fig. 4. CO $J = 1$–0 spectra toward star clusters harboring observed targets. The (0,0) positions correspond to the directions to St2-03, St2-18, Mc4-02, Mc8-03, Mc13-5. The (0,0) position in the last panel is toward 2MASS J18375890−0652321, F13 of Nakashima and Deguchi (2006) in Bica et al.'s #122. The offset positions were shown between the parentheses in arcsecond. The thick light blue bar in each panel indicates the possible velocity range of star clusters.

Galactic bulge, unlike the majority of usual star clusters formed in Galactic spiral arms.

4. Summary

We detected SiO maser emission ($J = 1$–0 $v = 1$ and 2) toward 11 out of 36 observed targets, including red supergiants and candidates for red supergiants in star clusters embedded in the Galactic disk. We also detected H_2O maser emission ($J_{KK} = 6_{16}$–5_{23}) in ten out of these 36 targets, of which both SiO and H_2O lines were detected in four. Accurate radial velocities of the detected objects were obtained from the velocities of SiO maser lines. The estimated kinematic distance indicates that the distance to Stephenson #2 is significantly smaller than that to Bica et al.'s #122. The radial velocity obtained from the present observation was used to check the association of CO gas with these clusters. We found that plenty of molecular gas still remains in Stephenson #2, whereas almost no molecular gas remains in Bica et al.'s #122. We conclude that the SiO and H_2O masers are useful tools for investigating massive stars in star clusters, and the kinematics of star clusters, as well as the mass-losing process of red supergiants. In the end, these studies will clarify detailed processes of disruption mechanisms of massive star clusters in the Galaxy.
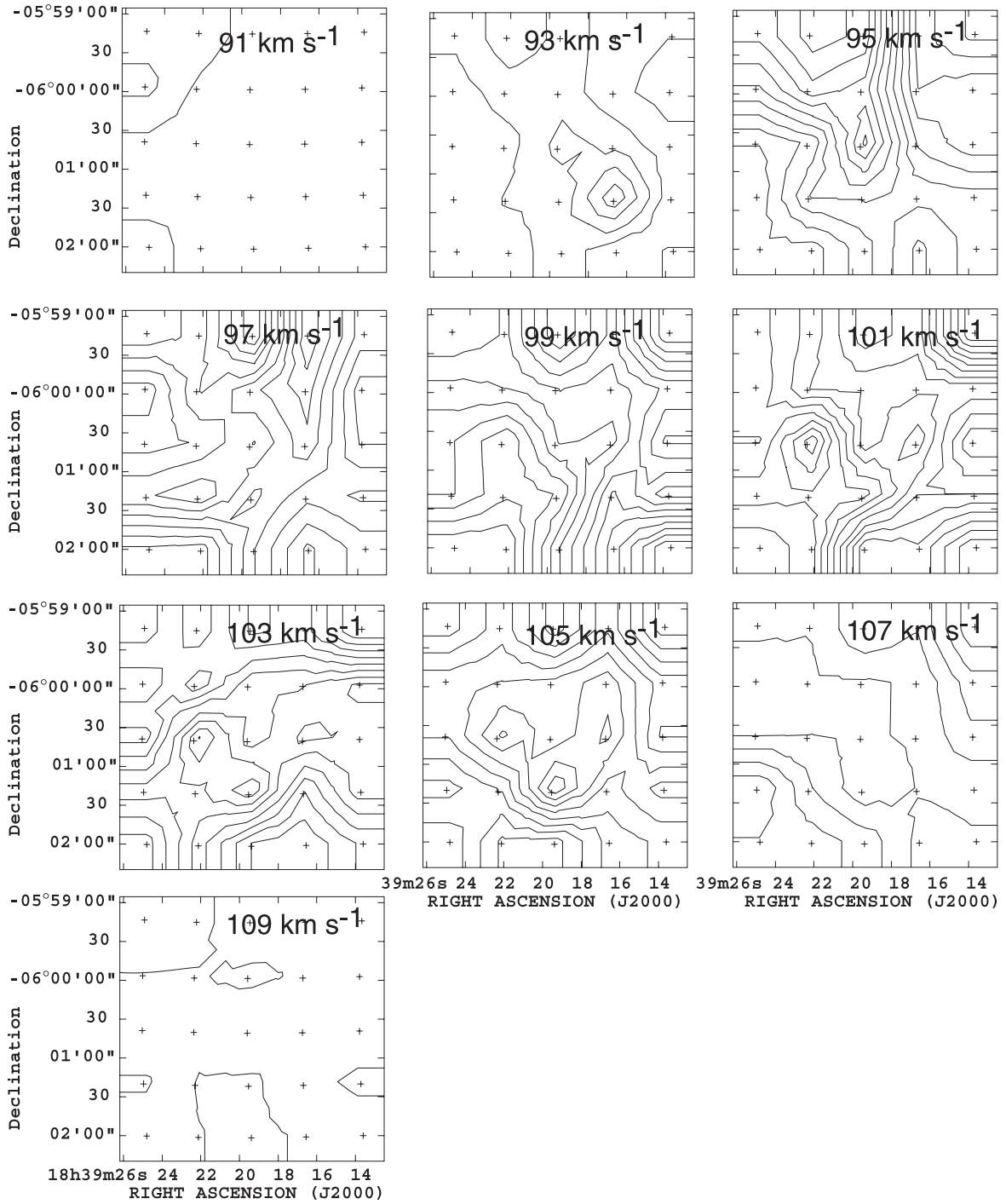
Fig. 5. (a) CO $J = 1$–0 channel maps toward Stephenson #2. Cross marks are positions observed with the array receiver. The contour levels are drawn every 0.3 K from the lowest one (0.3 K)
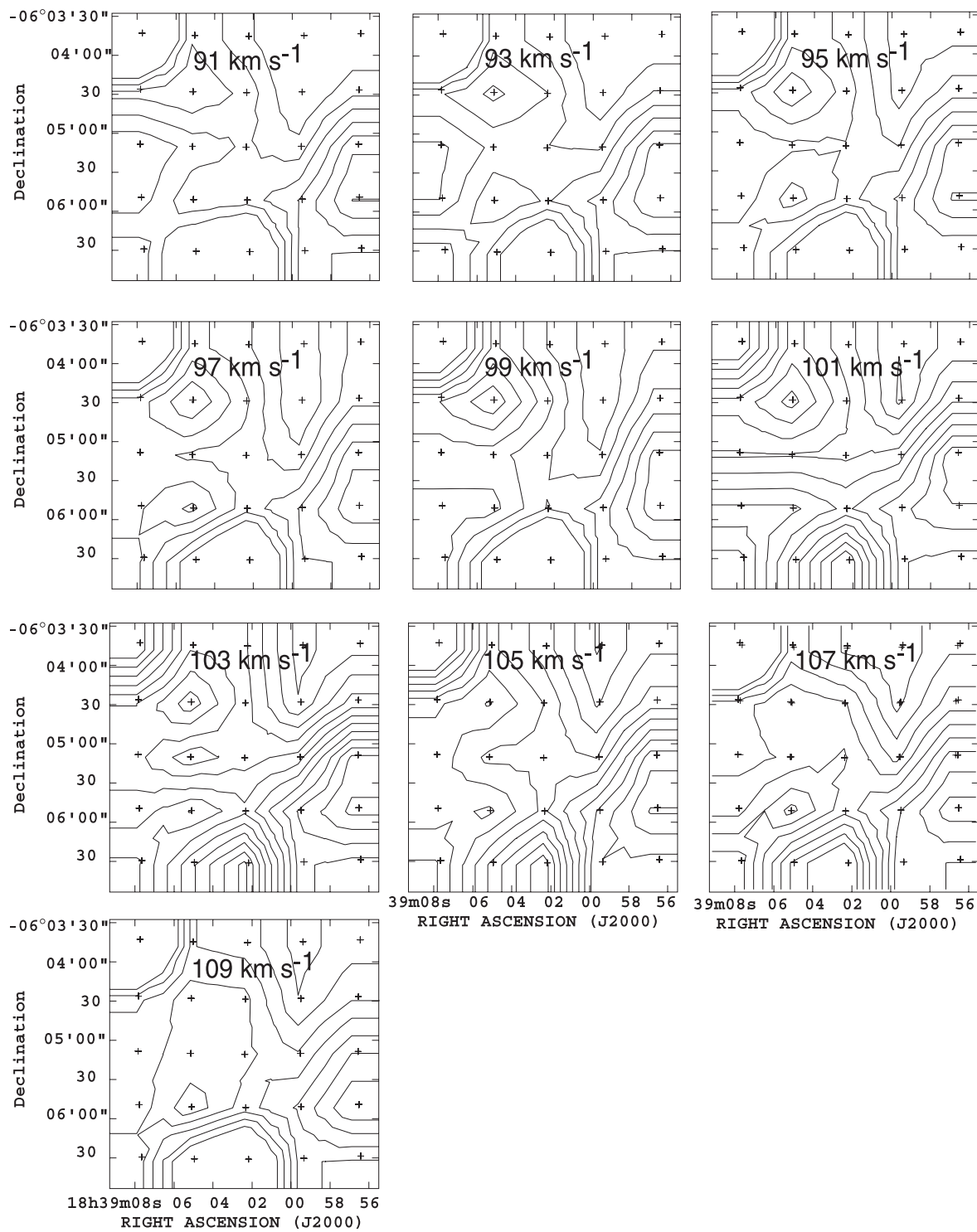
Fig. 5. (b) CO $J = 1$–0 channel map toward Stephenson #2 SW. Cross marks are positions observed with the array receiver. The contour levels are drawn every 0.5 K from the lowest one (0.5 K)
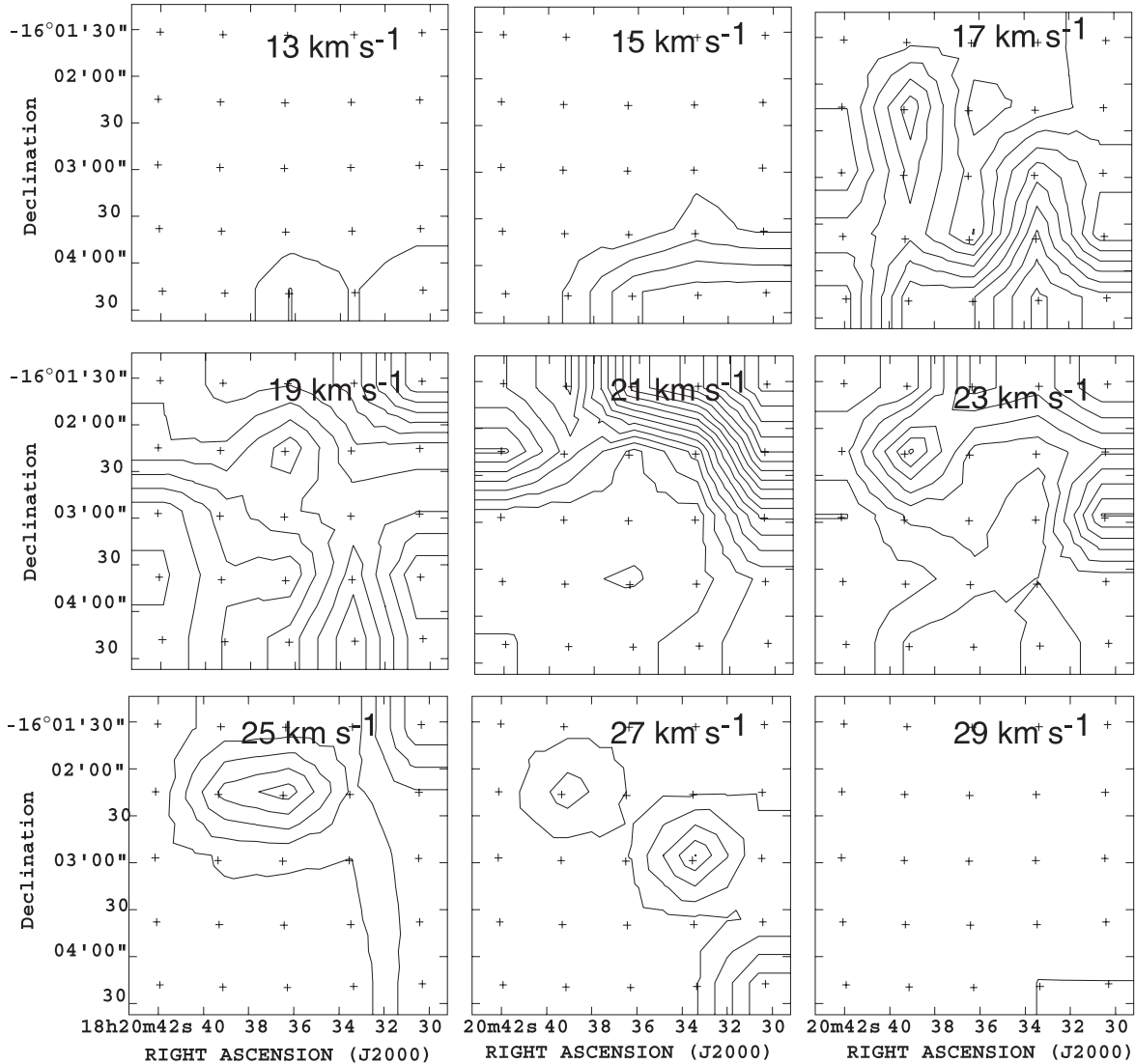
Fig. 5. (c) CO $J = 1$–0 channel map toward Mercer et al.'s #4. Cross marks are positions observed with the array receiver. The contour levels are drawn every 1.0 K from the lowest one (1.0 K)

which is a joint project of the University of Massachusetts and Infrared Processing and Analysis Center/California Institute of Technology, funded by the National Aeronautics and Space Administration and National Science foundation, and from the Midcourse Space Experiment at NASA/IPAC Infrared Science Archive, which is operated by the Jet Propulsion Laboratory, California Institute of Technology, under contract with the National Aeronautics and Space Administration.

Appendix. Individually Interesting Objects

- Mc4-02 (= M17WF 26): This star is located near the north boundary of M 17. Ando et al. (2002) studied infrared objects around M 17 and recorded that this star is designated as #26 in their table 2 (also see their figure 3). We detected SiO maser emission at $V_{\mathrm{lsr}} = 18\,\mathrm{km\,s^{-1}}$. The corrected K magnitude of this star is $K_{\mathrm{C}} = 5.45$. If the distance to this object is the same as that to M 17 (2.4 kpc) (Lada 1976), the luminosity

is estimated to be $\sim 10^3\,L_\odot$, which is too small to be a supergiant. The K_{s} magnitudes of this star measured in the past are 7.98 ± 0.02 (2MASS), 8.15 ± 0.05 (DENIS),[4] and 8.2 ± 0.2 (Ando et al. 2002). This star is possibly a distant bulge population, which has no direct relation to Mercer et al's #4.

- Mc8-01 (= IRAS 18258−1058): SiO masers were detected in this star by Izumiura et al. (1999) in their SiO maser survey of Galactic bulge stars. Deguchi et al. (1998) suggested a questionable NIR counterpart located $8''$ south of the IRAS position. However, the 2MASS star, J18283530−105636, which was identified in the present work, is much brighter, and is spatially closer to the MSX counterpart (G020.6034+00.0234). The SiO radial velocity ($\sim 74\,\mathrm{km\,s^{-1}}$) suggests that this object is not a member of Mercer et al.'s #8, and is possibly associated with the Galactic bulge.

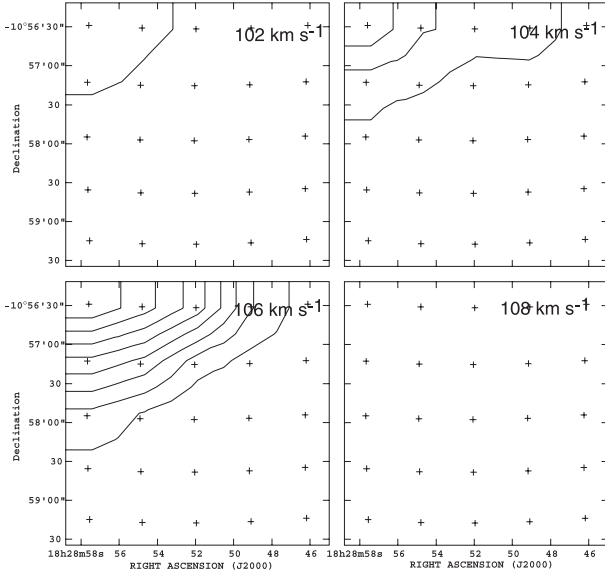4 ⟨http://cdsweb.u-strasbg.fr/denis.html⟩.

Fig. 5. (d) CO $J = 1$–0 channel map toward Mercer et al.'s #8. Cross marks are positions observed with the array receiver. The contour levels are drawn every 0.2 K from the lowest one (0.2 K)
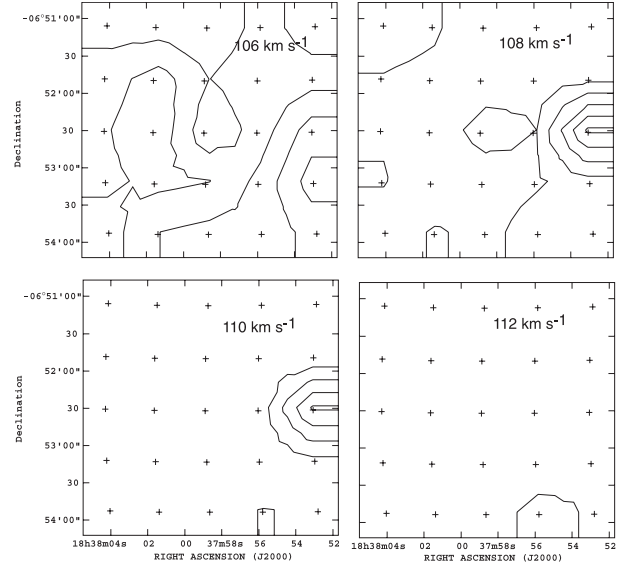

Fig. 5. (f) CO $J = 1$–0 channel map toward Bica et al.'s #112 (= RSGC1). Cross marks are positions observed with the array receiver. The contour levels are drawn every 0.2 K from the lowest one (0.2 K). No CO emission stronger than $T_a = 0.2$ K was found in channels of $V_{lsr} > 112$ km s^{-1}.
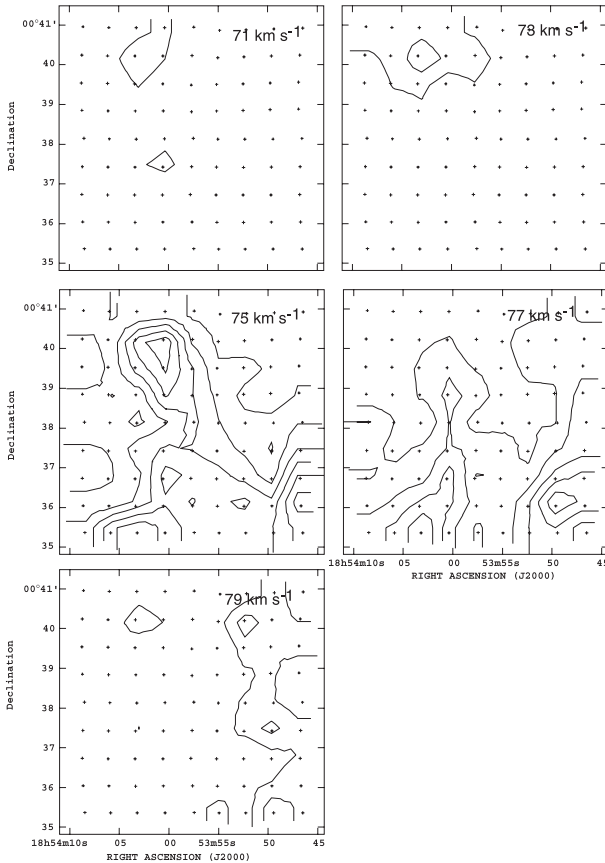

Fig. 5. (e) CO $J = 1$–0 channel map toward Mercer et al.'s #13. Cross marks are positions observed with the array receiver. The contour levels are drawn every 0.2 K from the lowest one (0.2 K).

- Mc13-1 (= IRAS 18511+0038): This object is an ultra-compact H II region (Giveon et al. 2007). In fact, CS $J = 7$–6 emission was detected toward this source at $V_{lsr} = 46$ km s^{-1} (Plume et al. 1992), though a search for the CS $J = 1$–0 and NH$_3$ (1, 1) lines was negative (Anglada et al. 1996). Water maser emission has been detected by Braz and Epchtein (1983) at $V_{lsr} = 38$ km s^{-1}, which is close to the peak velocity of 45.4 km s^{-1} obtained in this work. Since the large difference is found in the radial velocities, this object is not associated with Mercer et al.'s #13 which exhibits a radial velocity of ~ 72 km s^{-1}. No SiO maser was detected in this star.
- St2-03 (= IRAS 18366−0603): This object exhibits a relatively flat IRAS LRS spectrum with a small hump around 10 μm (Kwok et al. 1997). SiO and H$_2$O maser emissions were detected at $V_{lsr} = 103$ and 106 km s^{-1}, respectively, in the present observation. A search for the OH 1612 MHz maser was negative in a previous observation (IRC −10447: Wilson & Barrett 1972).
- St2-18 (= J18390238−0605106): This is an enigmatic object showing a K magnitude of 1.03 (corrected for interstellar extinction). IRAS LRS spectrum (IRAS 18363−0607) exhibits strong 10 and 18 μm silicate emission (Volk & Cohen 1989). Note that the typical K magnitude of SiO sources (AGB stars) in the Galactic bulge is ~ 5.5 (Fujii et al. 2006). It indicates that the luminosity of St2-18 is 30 times the luminosity of average bulge SiO sources at the K bands. An estimation of the luminosity by using the IRAS 12 and 25 μm flux densities (Jiang et al. 1996) gives a luminosity of $9 \times 10^4 L_\odot$ at a distance of 5.5 kpc.

References

Ando, M., Nagata, T., Sato, S., Mizuno, N., Mizuno, A., Kawai, T., Nakaya, H., & Glass, I. S. 2002, ApJ, 574, 187

Anglada, G., Estalella, R., Pastor, J., Rodríguez, L. F., & Haschick, A. D. 1996, ApJ, 463, 205

Benjamin, R. A. 2008, ASP Conf. Ser., 387, 375

Bica, E., Dutra, C. M., Soares, J., & Barbuy, B. 2003, A&A, 404, 223

Boily, C. M., & Kroupa, P. 2003, MNRAS, 338, 673

Braz, M. A., & Epchtein, N. 1983, A&AS, 54, 167

Cernicharo, J., Alcolea, J., Baudry, A., & González-Alfonso, E. 1997, A&A, 319, 607

Cesarsky, C. J., Cesarsky, D. A., Churchwell, E., & Lequeux, J. 1978, A&A, 68, 33

Dame, T. M., Hartmann, D., & Thaddeus, P. 2001, ApJ, 547, 792

Davies, B., Figer, D. F., Kudritzki, R.-P., MacKenty, J., Najarro, F., & Herrero, A. 2007, ApJ, 671, 781

Davies, B., Figer, D. F., Law, C. J., Kudritzki, R.-P., Najarro, F., Herrero, A., & MacKenty, J. W. 2008, ApJ, 676, 1016

Deguchi, S., et al. 2004a, PASJ, 56, 261

Deguchi, S., et al. 2004b, PASJ, 56, 765

Deguchi, S., Matsumoto, S., & Wood, P. R. 1998, PASJ, 50, 597

Egan, M. P., et al. 2003, Air Force Research Laboratory Technical Report AFRL-VS-TR-2003-1589[2]

Eigenbrod, A., Mermilliod, J.-C., Clariá, J. J., Andersen, J., & Mayor, M. 2004, A&A, 423, 189

Figer, D. F., MacKenty, J. W., Robberto, M., Smith, K., Najarro, F., Kudritzki, R. P., & Herrero, A. 2006, ApJ, 643, 1166

Fujii, T., Deguchi, S., Ita, Y., Izumiura, H., Kameya, O., Miyazaki, A., & Nakada, Y. 2006, PASJ 58, 529

Giveon, U., Richter, M. J., Becker, R. H., & White, R. L. 2007, AJ, 133, 639

Hall, P. J., Allen, D. A., Troup, E. R., Wark, R. M., & Wright, A. E. 1990, MNRAS, 243, 480

Heger, A., Fryer, C. L., Woosley, S. E., Langer, N., & Hartmann, D. H. 2003, ApJ, 591, 288

Izumiura, H., Deguchi, S., Fujii, T., Kameya, O., Matsumoto, S., Nakada, Y., Ootsubo, T., & Ukita, N. 1999, ApJS, 125, 257

Jackson, J. M., et al. 2006, ApJS, 163, 145

Jiang, B. W., Deguchi, S., Yamamura, I., Nakada, Y., Cho, S. H., & Yamagata, T. 1996, ApJS, 106, 463

Kwok, S., Volk, K., & Bidelman, W. P. 1997, ApJS, 112, 557

Lada, C. J. 1976, ApJS, 32, 603

Lada, C. J., & Lada, E. A. 2003, ARA&A, 41, 57

Lada, C. J., Margulis, M., & Dearborn, D. 1984, ApJ, 285, 141

Mercer, E. P., et al. 2005, ApJ, 635, 560

Nakashima, J., & Deguchi, S. 2006, ApJ, 647, L139

Nakaya, H., Watanabe, M., Ando, M., Nagata, T., & Sato, S. 2001, AJ, 122, 876

Ortolani, S., Bica, E., Barbuy, B., & Momany, Y. 2002, A&A, 390, 931

Plume, R., Jaffe, D. T., & Evans, N. J., II 1992, ApJS, 78, 505

Reid, M. J., & Dickinson, D. F. 1976, ApJ, 209, 505

Russeil, D. 2003, A&A, 397, 133

Salasnich, B., Bressan, A., & Chiosi, C. 1999, A&A, 342, 131

Schild, R. E. 1970, ApJ, 161, 855

Skrutskie, M. F., et al. 2006, AJ, 131, 1163

Sorai, K., Sunada, K., Okumura, S. K., Iwasa, T., Tanaka, A., Natori, K., & Onuki, H. 2000, Proc. SPIE, 4015, 86

Stephenson, C. B. 1990, AJ, 99, 1867

Sunada, K., Yamaguchi, C., Nakai, N., Sorai, K., Okumura, S. K., & Ukita, N. 2000, Proc. SPIE, 4015, 237

Van Blerkom, D., & Mao, X. 1982, ApJ, 252, L73

Volk, K., & Cohen, M. 1989, AJ, 98, 931

Wilson, W. J., & Barrett, A. H. 1972, A&A, 17, 385